Effects of monomer shape on the formation of aggregates from a power law monomer distribution

2013 New J. Phys. 15 073026

(http://iopscience.iop.org/1367-2630/15/7/073026)

New Journal of Physics
The open access journal for physics

Effects of monomer shape on the formation of aggregates from a power law monomer distribution

J Perry, J Kimery, L S Matthews[1] and T W Hyde
Center for Astrophysics, Space Physics and Engineering Research, Baylor University, Waco, TX 76798, USA
E-mail: Lorin_Matthews@Baylor.edu

New Journal of Physics **15** (2013) 073026 (14pp)
Received 16 January 2013
Published 15 July 2013
Online at http://www.njp.org/
doi:10.1088/1367-2630/15/7/073026

Abstract. The coagulation of dust aggregates is an important process in many physical systems such as the Earth's upper atmosphere, comet tails and protoplanetary discs. Numerical models which study the aggregation in these systems typically involve spherical monomers. There is evidence, however, via the polarization of sunlight in the interstellar medium, as well as optical and LIDAR observations of high-altitude particles in Earth's atmosphere (70–100 km), which indicate that dust monomers may not necessarily be spherical. This study investigates the influence of different ellipsoidal monomer shapes on the morphology of aggregates given various distributions of monomer sizes. Populations of aggregates are grown from a single monomer using a combination of ballistic particle–cluster aggregation and ballistic cluster–cluster aggregation regimes incorporating the rotation of monomers and aggregates. The resulting structures of the aggregates are then compared via the compactness factor, geometric cross-section and friction time.

[1] Author to whom any correspondence should be addressed.

Contents

1. Introduction

The coagulation of dust particles occurs in a variety of environments, such as the interstellar medium (ISM), protoplanetary discs (PPDs), Earth's upper atmosphere and industrial processes (Ossenkopf and Henning 1994, Dullemond and Dominik 2005, Bardeen *et al* 2008). Aggregates within these environments are believed to grow via collisions between micron and sub-micron sized dust particles, forming larger structures called aggregates (Blum and Wurm 2008). It is therefore essential to understand the manner in which particles interact and how their structure depends upon the physical parameters of the particles themselves and their environment. A detailed study of the micro-physics that governs interparticle forces as well as the evolution of aggregate structures during and after collisions is a key component in accurately modeling the evolution and behavior of the dust populations within these environments.

A number of computer models have been employed to date which explore the behavior of interacting and colliding dust grains under various conditions (Dominik and Tielens 1997, Dominik and Nubold 2002, Matthews and Hyde 2004, 2008, 2009, Matthews *et al* 2007, 2012, Wada *et al* 2007, 2008, 2009, 2011, Suyama *et al* 2008, 2012, Paszun and Dominik 2009, Perry *et al* 2010). A near ubiquitous assumption in these models is the use of spherical monomers as the building blocks of larger aggregates.

When individual grains come into contact they are held together through attractive forces at their surfaces. The lower limit of this attractive force is given by van der Waals attraction, but other forces, such as dipole–dipole interactions between icy or metallic grains, may be involved, depending on the materials (Dominik and Tielens 1997). In a comprehensive model, the specific chemistry of the dust particles must be considered in order to account for differing behavior due to grain material. Many experiments have dealt with the collision properties of silica or silicates as relevant grain materials for dust agglomeration at 1 AU (see Blum and Wurm (2008) for an overview), though organics (Kouchi *et al* 2002), ices (Bridges *et al* 1996) and magnetic materials (Nubold *et al* 2003) have also been considered. Since in astrophysical systems, grains exist in a plasma or radiative environment, grains may also become charged, leading to attractive or repulsive forces between monomers. Based on the surface chemistry and interactions, not all collisions will result in pure sticking. It is necessary to understand the effects of all these parameters, and more, to develop a complete model of aggregation.

In this study, we examine the effect of monomer shape on grain morphology. Some observational evidence suggests deviation from a simple spherical structure. Polarization of

sunlight scattered by cometary dust suggests the presence of dust monomers having a major axis three times longer than their minor axis (Hage and Greenberg 1990). Indications of non-spherical monomers may also be found in the Earth's upper atmosphere, at altitudes of 70–100 km, where tons of meteoric material is ablated by heat and friction during each rotational period (Gabrielli *et al* 2004). This ablated material, termed meteoric smoke particles, has been conjectured to play an important role in atmospheric processes, such as the nucleation of ice particles, and in polar summer mesospheric echoes (Keesee 1989). Optical analysis (considering aspheric monomers) of recent ground based Light Detection and Ranging (LIDAR) measurements of meteoric smoke particles has found that the aspect ratio of these monomers may vary from 0.1 to 10 (Baumgarten *et al* 2007).

Recently, a study was conducted to examine the impact monomer shape has on ballistic aggregation, comparing results for models using prolate ellipsoids with an aspect ratio of 3:1:1 and spherical monomers (Perry *et al* 2012). Aggregates were built using monodisperse monomers under both ballistic particle–cluster aggregation (BPCA) and ballistic cluster–cluster aggregation (BCCA) collision regimes and the resulting morphologies were examined. Aggregates of these two types of monomers were seen to differ structurally as they grew to large size. Ellipsoidal monomers tended to form aggregates which were more compact under BCCA collisions; this in turn led to these aggregates being less well-coupled to the local gas environment, as indicated by longer friction times. At sizes of about 300 monomers, aggregates built from ellipsoidal monomers had friction times double that of aggregates built from spherical monomers, with a much wider distribution for a given size. It must therefore be considered that monomer shape may play an important role as a free parameter when examining the evolution of the dust population.

This study expands upon this previous work in two ways: (i) additional aspect ratios are explored, including oblate ellipsoids in addition to prolate ellipsoids and (ii) aggregates are built from polydisperse monomer populations, reflecting size distributions found in astrophysical environments (Mathis *et al* 1977, Martin and Whittet 1990).

2. Methods

In this study, creation of aggregates occurs by simulating pair-wise interactions of dust particles (here particle refers to either a monomer or an aggregate consisting of two or more monomers). The model used has previously been employed to examine the coagulation of charged dust particles, coagulation considering the influence of magnetic materials, as well as coagulation of ellipsoidal monomers (Matthews and Hyde 2008, Perry *et al* 2010, 2012, Matthews *et al* 2012). The model was modified to allow the monomer axes to be set to any desired aspect ratio, permitting various ellipsoidal shapes to be examined, such as the prolate and oblate ellipsoids used in this study. The monomer distribution was also modified to follow a power-law size distribution characterized by $n(r) \propto r^{-\alpha}$, where r is the semi-major axis (or radius) of a monomer and α is an exponent which determines the slope of the size distribution.

Three monomer shapes were selected for study. Spherical monomers were initially employed to establish control populations for comparison. Then prolate ellipsoidal monomers (with one semi-major axis and two equal semi-minor axes) and oblate ellipsoidal monomers (with two equal semi-major axes and one semi-minor axis) were examined. The maximum and minimum radii used in each model were varied to maintain a constant volume and mass for

Table 1. Aspect ratio and size range for monomer shapes used as building blocks for aggregates grown through ballistic collisions.

Monomer shape	Aspect ratio	Radii (μm)
Spherical	1:1:1	0.120–2.404
Prolate ellipsoidal	3:1:1	0.250–5.000
	5:1:1	0.351–7.029
	10:1:1	0.558–11.16
Oblate ellipsoidal	3:3:1	0.173–3.460
	5:5:1	0.206–4.110
	10:10:1	0.259–5.179

monomers across all simulations. Monomer shapes, aspect ratios and radii (semi-major axes) for all populations are shown in table 1.

Two representative values of α, $\alpha = 1.8$ and 3.5, were used in this study. Observations of the ISM in the near- and mid-IR ranges have suggested dust size distributions with power-law exponent as low as $\alpha = 1.8$, while observations taken in the UV and visible spectrum suggest size distributions having exponents as large as $\alpha = 3.5$ (Mathis *et al* 1977, Martin and Whittet 1990). Monodisperse populations, i.e. $\alpha = \infty$, were also modeled for the smallest and largest possible monomer sizes for each shape tested.

Aggregates begin as a single monomer which is placed at the origin of the coordinate system. A new particle is generated at a random position $20R$ away from the target particle, where R is the maximum radius of the target monomer or aggregate measured from its center of mass (COM). Particles are also given a random initial orientation, important for non-spherical monomers. Particle trajectories are directed toward the COM of the initial particle with an offset ranging from 0 to $\frac{1}{2}(R_1 + R_2)$, or half the sum of the radii of the two particles. As an incoming particle approaches within a distance $(R_1 + R_2)$, the closest two monomers in each aggregate are examined to determine when overlap occurs. In the low-velocity regime employed here, monomers are assumed to stick at their point of contact and be held together via van der Waals forces without the possibility of rolling or sliding (Dominik and Tielens 1997).

In contrast to previous N-body simulations which defined BCCA as collisions between clusters of the same size, such as Meakin (1991), collisions for a continuous range of mass ratios are sampled. This method is similar to quasi-BCCA (QBCCA), in which collisions between two aggregates with a fixed mass ratio are modeled (Okuzumi *et al* 2009). First generation aggregates ($N \leqslant 20$) are grown through BPCA collisions where each incoming particle is a single monomer. After a collision, the new aggregate's characteristic parameters (mass, spin, etc), are calculated and stored in a library for later analysis and use. The newly created aggregate then becomes the target for the subsequent collision. Second and third generation aggregates, $(20 < N \leqslant 200)$ and $(200 < N \leqslant 2000)$ respectively, are grown through BCCA collisions, with the target aggregate and the incoming aggregate being randomly selected from the libraries of previous generation(s). In this manner, collisions between all possible mass ratios are sampled, which offers a small improvement over QBCCA which models collisions between two clusters with fixed mass ratios (Okuzumi *et al* 2009). The limit of $N = 20$ was chosen for the first generation of aggregates since the parameters which characterize their fractal nature

(fractal dimension, compactness factor) are not well-defined for particles with fewer than ∼10 monomers. The second and third generation cutoffs, $N = 200$ and 2000, increase the terminal particle size by a factor of 10. Changing these bounds does not significantly alter the final results, as the plots of all of the aggregate characteristics can be seen to have continuous slopes across these boundaries.

Aggregate morphologies are compared using the physical characteristics of the aggregates, such as the compactness factor and the radius of the geometric cross-section, R_σ, as well as the friction time, a parameter characterizing interactions with the gas environment. Each of these is described below.

2.1. Compactness factor

The compactness factor is a measure of the openness, often referred to as the 'fluffiness', of an aggregate. Lower compactness factors indicate a more open aggregate structure, while a higher compactness factor is indicative of a more compact morphology, approaching a limiting value of one for spherical aggregates. Aggregates with very open structure have higher cross-sectional areas, thus increasing the probability of additional collisions.

The compactness factor is defined as the ratio of the volume of the constituent monomers to the volume of a sphere with a radius determined by the average projected cross-section of the aggregate, A_σ. Thus, the compactness factor is given by

$$\Phi_\sigma = \frac{\Sigma_i r_i^3}{R_\sigma^3}, \tag{1}$$

where r_i is the radius of the ith monomer and the sum runs over all the monomers in the aggregate, and R_σ is the radius of a circle with area equal to the projected cross-section, averaged over numerous orientations to minimize variance (Paszun and Dominik 2009). For an ellipsoid, $r_i^3 = abc$, where a, b and c are the semi-axes of the monomer.

2.2. Friction time

The friction time of an aggregate indicates how strongly a particle is coupled to the gas in which it is immersed; a short friction time indicates a well-coupled aggregate. The friction time of an aggregate is given by

$$\tau_\mathrm{f} = \frac{m}{\sigma}\frac{1}{\rho_\mathrm{g} v_\mathrm{th}}, \tag{2}$$

where m is the mass of the aggregate, σ is the cross-sectional area of the aggregate averaged over many orientations, ρ_g is the density of the gas and v_th is the thermal sound speed (Armitage 2010). Relative velocities between aggregates depends on the difference in their friction times (Ormel and Cuzzi 2007, Matthews *et al* 2012).

3. Results

A sampling of aggregates grown assuming ballistic collisions under the conditions previously described is shown in figure 1. The physical characteristics for aggregates formed from each of the monomer population types were analyzed, with the results presented in this section representing averages for the data binned by mass, normalized by the minimum monomer mass,

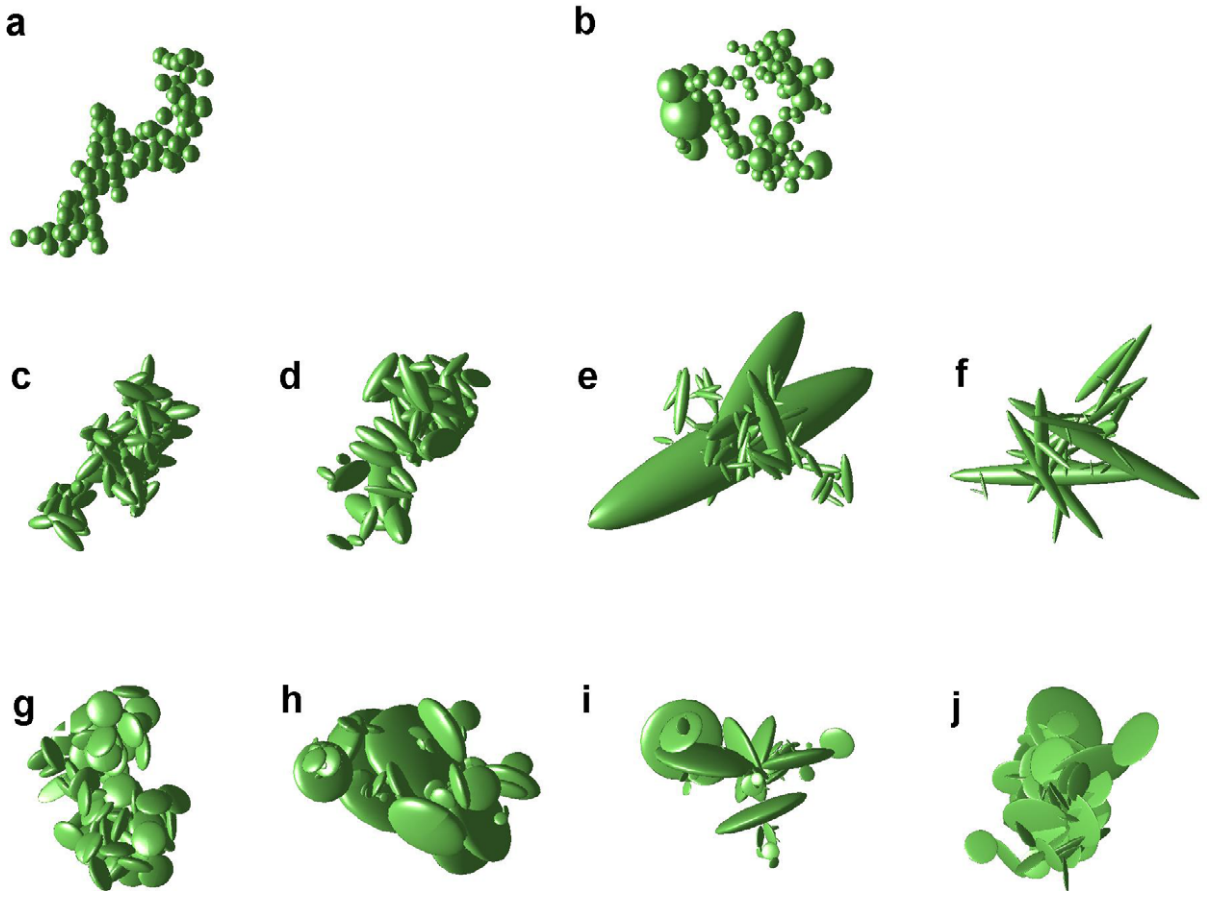

Figure 1. Sample aggregates grown from populations using the method described in section 2. Each aggregate contains ≈80 monomers using (a), (c) and (g) monodisperse spheres, prolate ellipsoids (3:1:1), and oblate ellipsoids (3:3:1), (b) polydisperse spheres, (d)–(f) polydisperse prolate ellipsoids with axis ratios (3:1:1), (5:1:1) and (10:1:1) respectively, and (h)–(j) polydisperse oblate ellipsoids with axis ratios (3:3:1), (5:5:1) and (10:10:1) respectively.

m/m_0, or number of monomers, N. Under the ballistic aggregation regimes employed, the two monodisperse populations were found to have nearly equivalent values for the characteristics examined, so for clarity only the results for the larger size monodisperse populations are shown in figures 2–6.

The radius of the average geometric cross-section, R_σ, grows via a power law, ($R_\sigma \propto (\frac{m}{m_0})^\beta$), as shown in figure 2. As the aggregates grow larger in size ($N \geqslant 20$), the radius of the average geometric cross-section, R_σ, trends to a power-law dependence on the mass. Here R_σ has been normalized by the smallest average monomer radius for each population. Independent of the monomer sizes and distributions, aggregates comprised of spherical monomers, on average, have a radius which grows faster with mass than do aggregates comprised of either type of ellipsoidal monomers, as measured by the slope of the fit line to the data. The simplest reason for this is that ellipsoidal shapes can pack more efficiently than spheres, as is also reflected in the larger compactness factors seen for ellipsoids. Comparing aggregates composed of ellipsoidal

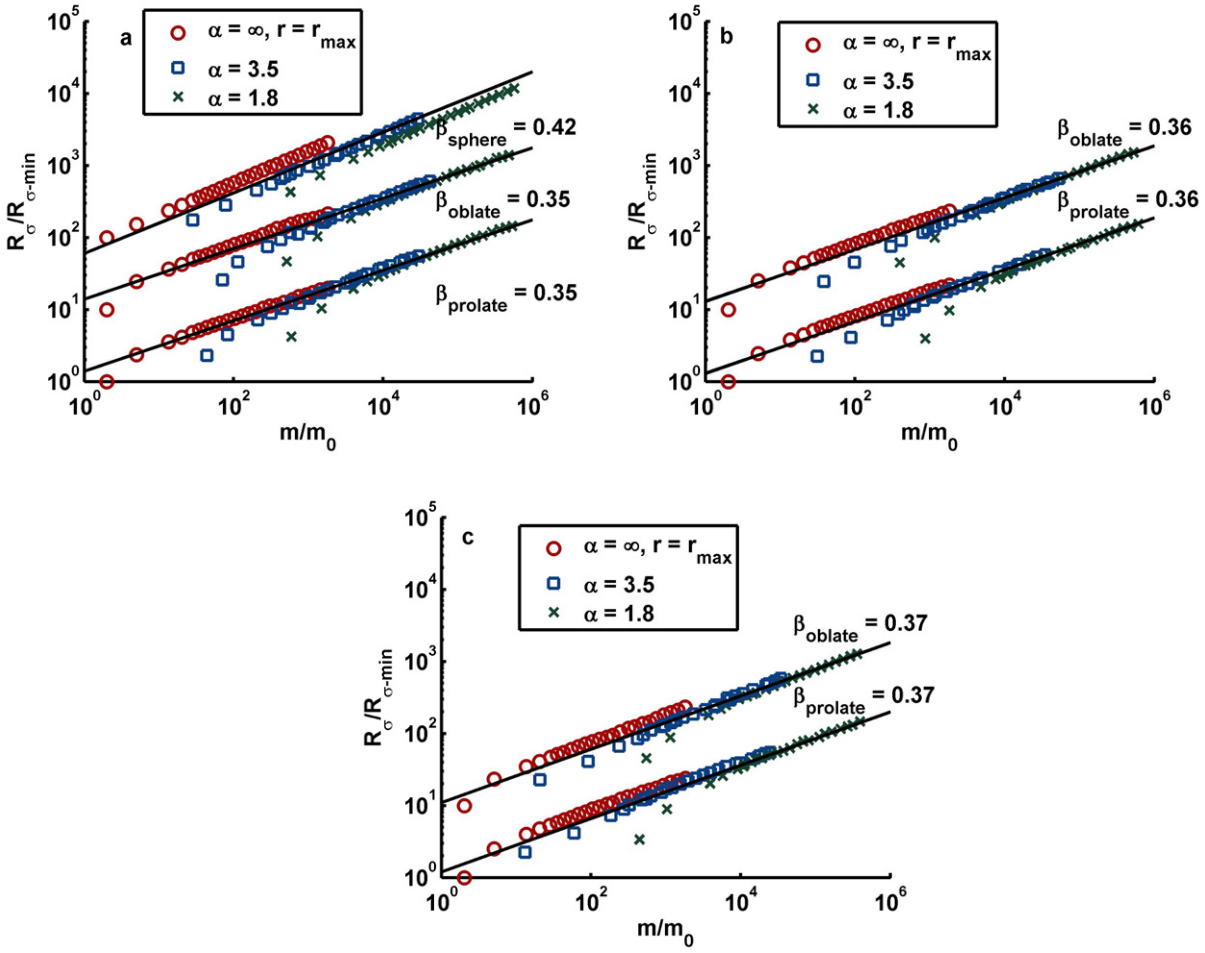

Figure 2. Average R_σ versus mass for aggregates built from the larger monodisperse population and two different polydisperse populations. The solid line shows the trend for aggregates with $N \geqslant 20$ for the combined populations for each monomer shape. The slope, β, is indicated for (a) spheres and ellipsoids with aspect ratios of (3:1), (b) ellipsoids with aspect ratios of (5:1), and (c) ellipsoids with aspect ratios of (10:1). For clarity, oblate and spherical populations have been offset by $\times 10$ and $\times 100$ respectively.

monomers, it is seen that prolate and oblate shapes having the same aspect ratio both form aggregates which grow via the same power law exponent. It is interesting to note that the exponent does not vary much as the aspect ratio is increased, and that the monodisperse and power law distributions can be fit by the same trend line. Due to the logarithmic binning of the data, the fit lines are weighted toward the larger aggregates. The largest deviations from a single fit line are seen for spheres; however, the small aggregates in all populations have large deviations from the fit line which has interesting consequences for the friction times, shown in figure 6.

Aggregates built from ellipsoidal monomers (figures 3(b)–(g)) are initially less compact than those built from spheres, a direct result of ellipsoidal monomers having a smaller compactness factor than spherical monomers. However, as these aggregates grow they quickly

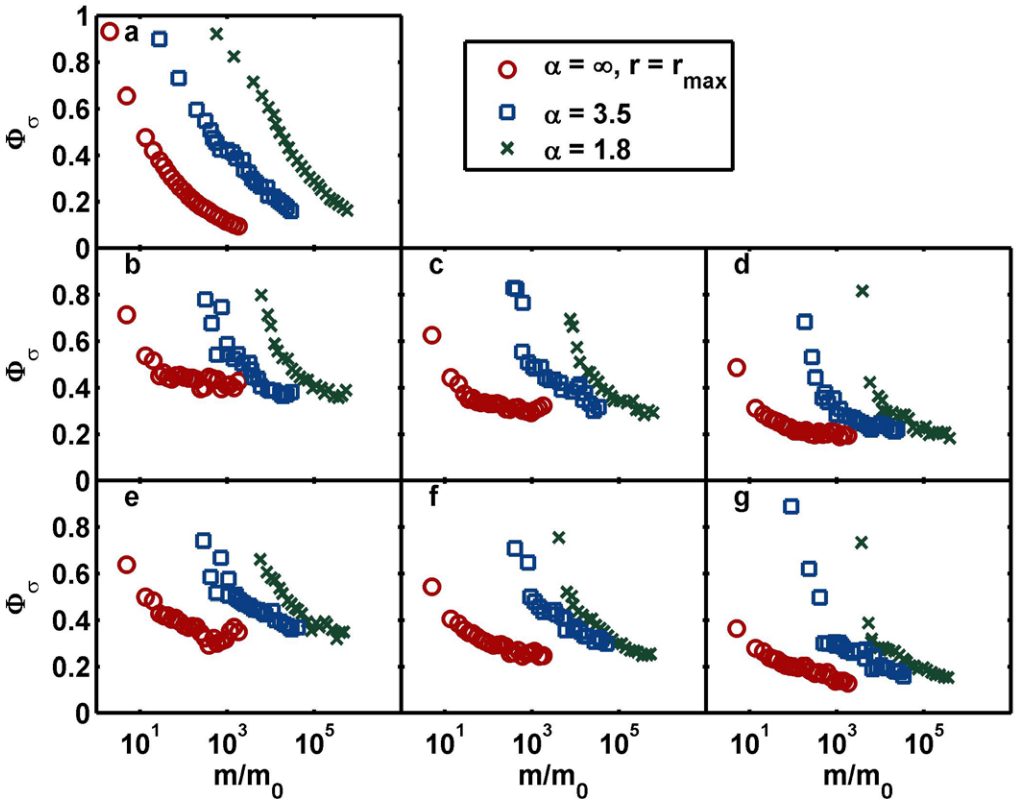

Figure 3. Average compactness factors versus normalized mass for aggregates built from the larger monodisperse population and two different polydisperse populations for (a) spherical monomers, (b)–(d) ellipsoidal prolate monomers with aspect ratios of (3:1:1), (5:1:1) and (10:1:1) respectively, and (e)–(g) ellipsoidal oblate monomers with aspect ratios of (3:3:1), (5:5:1) and (10:10:1) respectively.

approach a lower limit for the compactness factor, which in all cases is greater than that for spheres. The minimum compactness factor decreases as the aspect ratio increases, a trend that can be seen for aggregates formed from both prolate (figures 3(b)–(d)) and oblate (figures 3(e)–(g)) ellipsoids.

Examining the compactness factor as a function of N provides additional insight into aggregate growth. Data for second and third generation aggregates ($20 \leqslant N < 2000$) are shown in figure 4. As in figure 3, aggregates built from spheres (figure 4(a)) tend to be less compact than those built from ellipsoids (figures 4(b)–(g)). It is interesting to note that the monodisperse populations (denoted by the circles in all figures) have a smaller range of compactness factors, with this range tending to decrease as the aspect ratio of the ellipsoidal monomers increases. At the largest values of N, aggregates built from monodisperse and polydisperse monomer populations tend to have similar compactness factors, with the monodisperse populations tending to be slightly more fluffy. The one exception to this is seen for the prolate ellipsoids (3:1:1) (figure 4(b)).

The trend of ellipsoidal monomers to have maximum compactness factors for the smallest aspect ratios may be attributed to the packing efficiency of these shapes. It has been shown

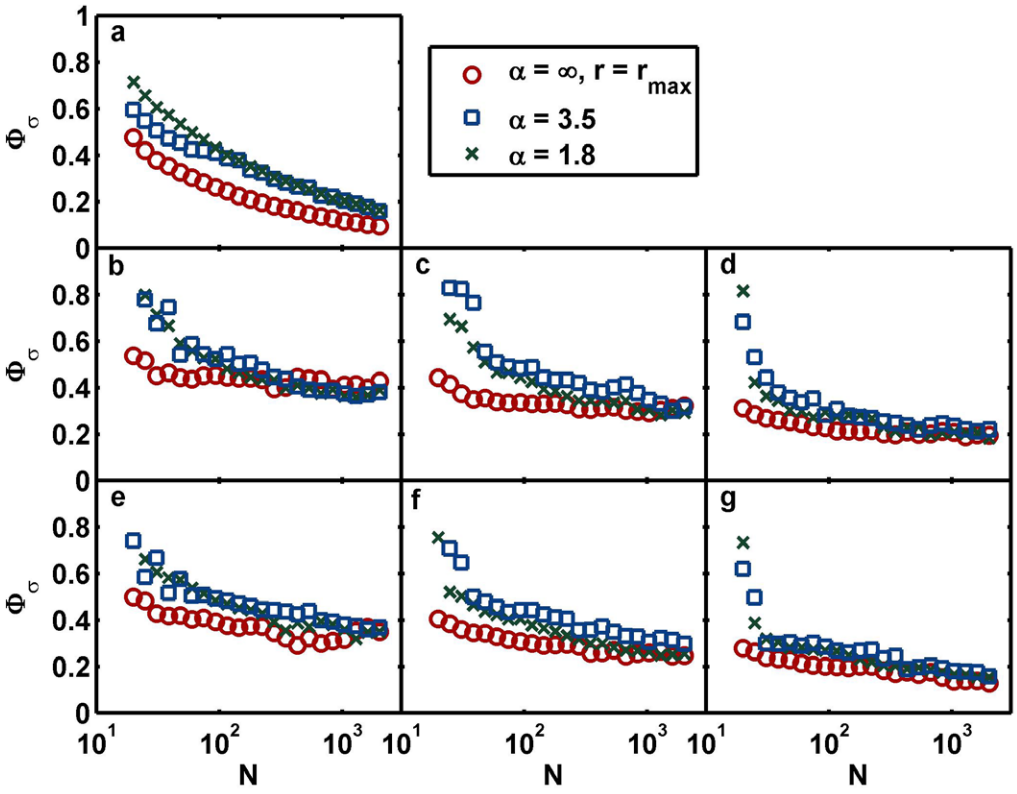

Figure 4. Average compactness factors versus number of monomers for second and third generation aggregates for (a) spherical monomers: (b)–(d) ellipsoidal prolate monomers with aspect ratios of (3:1:1), (5:1:1) and (10:1:1) respectively; and (e)–(g) ellipsoidal oblate monomers with aspect ratios of (3:3:1), (5:5:1) and (10:10:1) respectively.

numerically that as the aspect ratio changes from 1:1:1, the packing efficiency initially increases, reaching a maximum at an aspect ratio of 1.5:1:1 for prolate ellipsoids and 2.5:2.5:1 for oblate ellipsoids, and then steadily decreases. However, the packing efficiency for ellipsoids is always greater than that for spheres (Donev *et al* 2004). Therefore the higher compactness factors seen for the prolate (3:1:1) and oblate (3:3:1) ellipsoids, figures 3(b) and (e), 4(b) and (e), are due to these shapes being the most space efficient monomer shapes modeled, while the larger aspect ratios have reduced packing efficiency.

Additional information on the evolution of the morphology of aggregates may be gleaned from the compactness factor by examining the standard deviations from the mean values, which were omitted from figures 3 and 4 for the sake of clarity. Scaled standard deviation, $\sigma/\bar{\Phi}_\sigma$, versus scaled mass has been plotted in figure 5 for both monodisperse and polydisperse populations. Here a clear difference can be seen between aggregates built from spheres and ellipsoids. Spherical monomers (denoted by circles in figures 5(a)–(c)) tend to build self-similar aggregates with small deviations from the mean compactness factor (minimum deviation on the order of 5%). Polydisperse spheres lead to small aggregates having larger deviations, which decrease as the aggregate mass grows (figures 5(b) and (c)). Aggregates built from ellipsoidal monomers, on the other hand, have larger deviations from the mean which remain

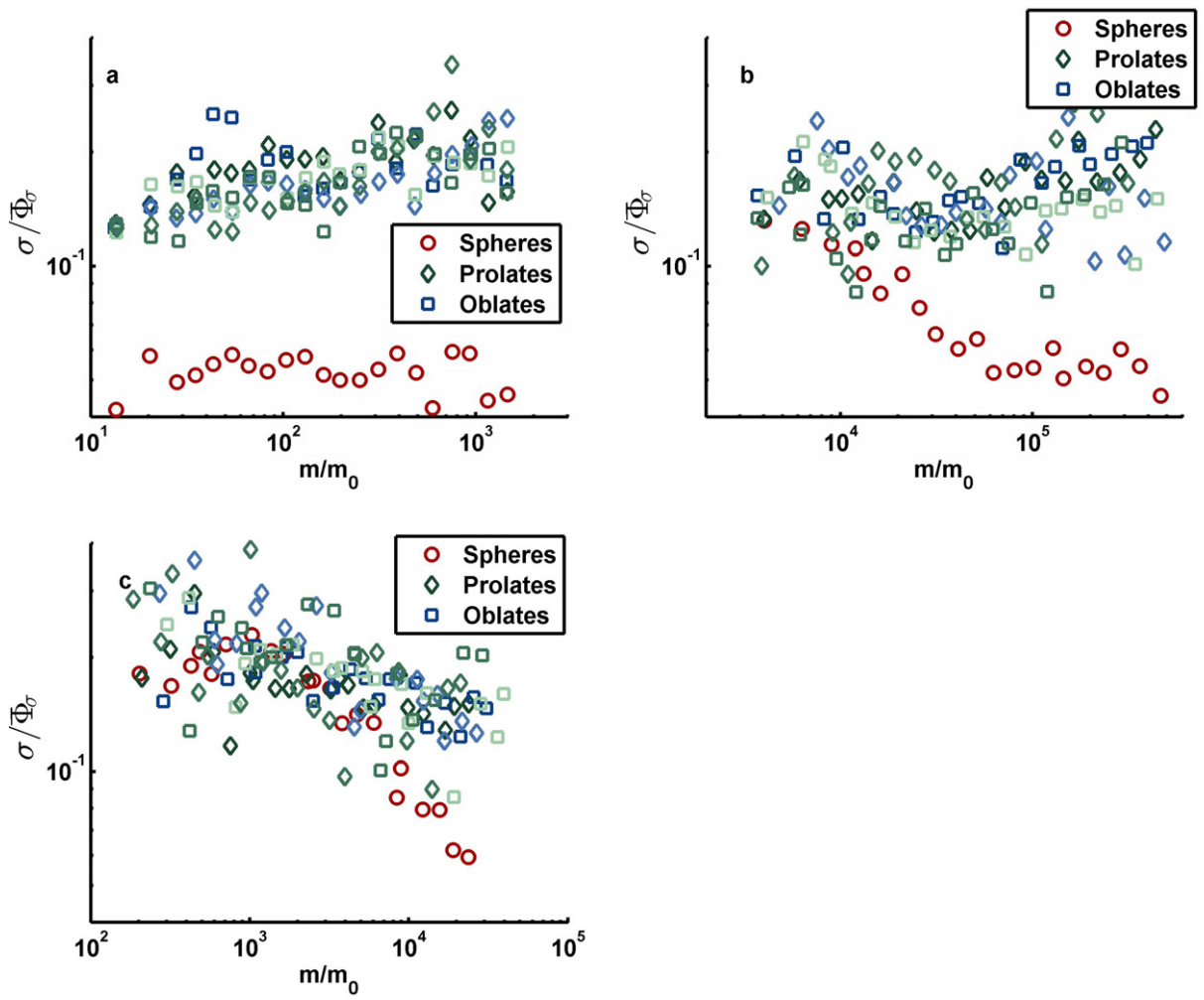

Figure 5. Standard deviations scaled by the average compactness factor versus scaled masses for (a) monodisperse populations, (b) polydisperse populations with $\alpha = 1.8$ and (c) polydisperse populations with $\alpha = 3.5$. For the prolate and oblate populations, the darkest markers correspond to aspect ratios of 3:1, the medium shade corresponds to aspect ratios of 5:1, while the lightest shade denotes aspect ratios of 10:1.

relatively constant (for monodisperse populations, figure 5(a)) or even increase (polydisperse population with $\alpha = 1.8$, figure 5(b)) as aggregate mass increases. The greatest deviations are understandably seen for the polydisperse populations with $\alpha = 3.5$ (figure 5(c)), though spherical monomers still tend to lead to smaller deviations which decrease the most rapidly with increasing mass. For ellipsoids, all aspect ratios selected for this study tend to deviations of $\sigma/\bar{\Phi}_\sigma = 0.1 - 0.3$.

Friction times, normalized by the minimum monomer response time, τ_{min} within a given population, as a function of normalized mass, are shown in figure 6. Aggregates built from spherical monomers have friction times which vary minimally as aggregates increase in size (figure 6(a)). The normalized friction times for the monodisperse spheres agree well with

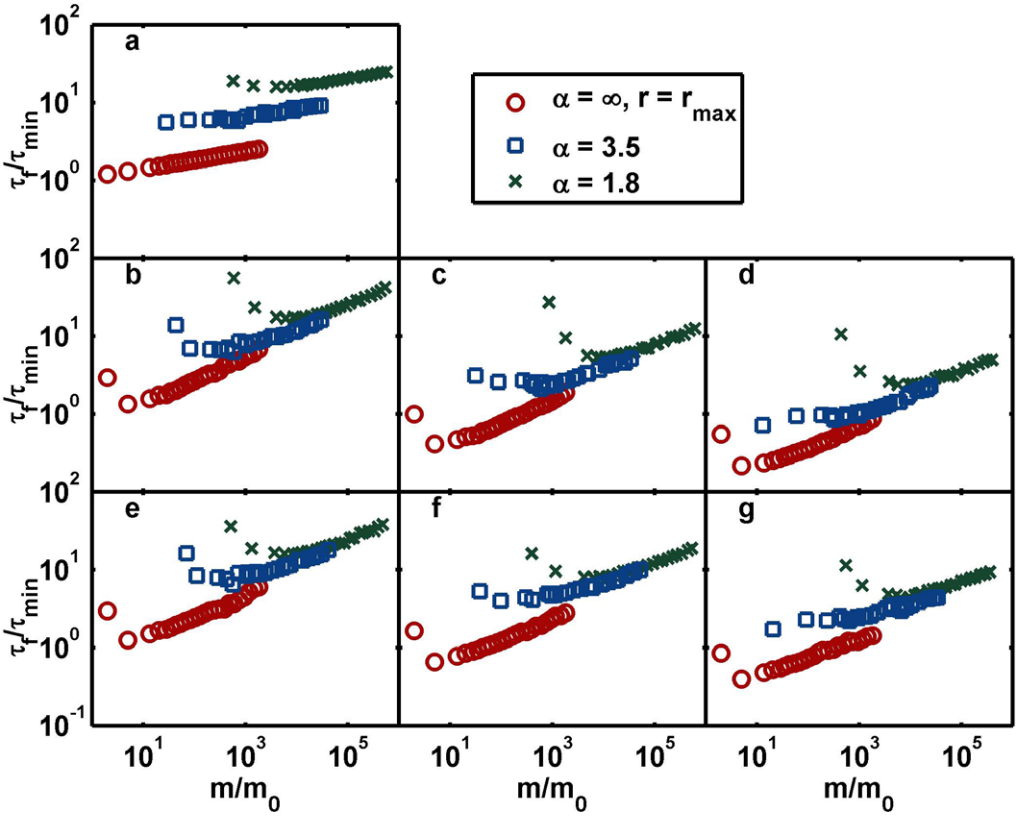

Figure 6. Normalized friction times versus normalized mass for aggregates built from the larger monodisperse population and two different polydisperse populations for (a) spherical monomers; (b)–(d) ellipsoidal prolate monomers with aspect ratios of (3:1:1), (5:1:1) and (10:1:1) respectively; and (e)–(g) ellipsoidal oblate monomers with aspect ratios of (3:3:1), (5:5:1) and (10:10:1) respectively.

the results for the mass-to-area ratio presented in Okuzumi *et al* (2009). The friction times predicted by this model, with a continuous range of mass ratios for colliding aggregates, agree most closely with that for collisions with a fixed mass ratio of $\epsilon = 0.1$. By comparison, aggregates built from ellipsoidal monomers have higher friction times which initially decrease with mass, then increase (more rapidly than for the aggregates with spherical monomers). From figures 6(b)–(g) it is seen that the trends for friction times vary most strongly with the aspect ratio of the monomers themselves, not simply the monomer shape. For aspect ratios of 3:1 (figures 6(b) and (e)) the friction times have the steepest slope for larger aggregates; they also produce the most pronounced 'bowl-shaped' minimum for mid-sized aggregates formed from polydisperse populations. Aggregates built from monomers with aspect ratios of 5:1 (figures 6(c) and (f)) or 10:1 (figures 6(d) and (g)), have friction times which increase more slowly with a shallower 'bowl', especially as α increases.

Further details about the response of aggregates to their environment may be seen by examining the standard deviation from the mean friction times, which were omitted from the previous figure for clarity. Scaled standard deviation, $\sigma/\bar{\tau}_f$, versus normalized mass is shown in figure 7 for both monodisperse and polydisperse populations. For monodisperse

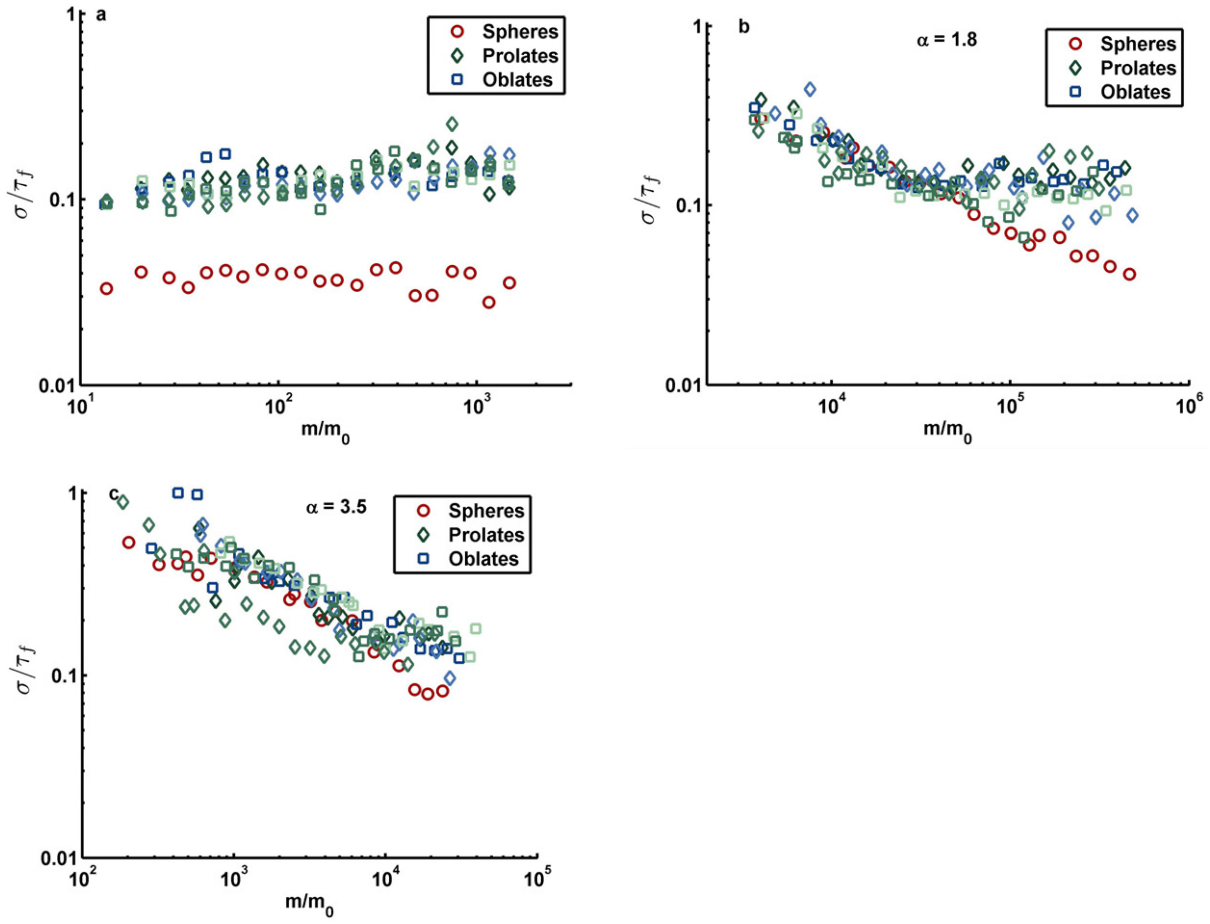

Figure 7. Standard deviations scaled by the average friction time versus normalized mass for (a) monodisperse populations, (b) polydisperse populations with $\alpha = 1.8$ and (c) polydisperse populations with $\alpha = 3.5$. For the prolate and oblate populations, the darkest markers correspond to aspect ratios of 3:1, the medium shades to aspect ratios of 5:1, while the lightest shades denotes aspect ratios of 10:1.

populations, figure 7(a), aggregates built from spheres show a much lower deviation than ellipsoidal monomer populations, though all monomer types lead to deviations which are relatively constant with mass. The standard deviation for polydisperse populations tends to decrease with aggregate size (figures 7(b) and (c)). As mass increases, the spherical monomers produce smaller deviations from the mean friction time than aggregates composed of ellipsoidal monomers. Thus, aggregates composed of ellipsoidal monomers will typically have a broader range of friction times, especially at large sizes, producing a wider possible response to turbulence leading to varying relative velocities and enhanced collision probabilities.

4. Discussion and conclusion

Aggregates were grown using both BPCA and BCCA methods for three different monomer shapes: spheres, prolate ellipsoids with aspect ratios of 3:1:1, 5:1:1 and 10:1:1, and oblate

ellipsoids with aspect ratios of 3:3:1, 5:5:1 and 10:10:1. Aggregates were assembled from monomers obeying a size distribution $n(r) \propto r^{-\alpha}$ for polydisperse distributions with $\alpha = 1.8$ and 3.5, as well as two monodisperse cases, corresponding to $\alpha = \infty$, each using the smallest and largest monomer radii for each shape. The structure of the resulting aggregates was compared according to aggregate radius, compactness factor and friction time.

Deviation from the standard assumption of spherical monomers for modeling dust coagulation was shown to have a definitive impact on the overall aggregate structure (characterized by the compactness factor) and the relative velocities (characterized by the friction time) for aggregates in astrophysical environments. Ellipsoidal monomers form aggregates which are more compact (less fluffy, figures 3 and 4), have smaller equivalent radii (figure 2), and exhibit a wider range of response times to turbulent eddies (figure 6) than do aggregates grown from spherical monomers.

Even so, the wide variation in structure and friction times seen for aggregates of a given size built from ellipsoids may make coagulation more efficient, as large aggregates can still have relatively large differences in relative velocities with each other (figure 7), which drives collisions. On the other hand, large aggregates built from spheres tend to have similar friction times, which leads to small relative velocities, eventually halting aggregate growth.

5. Future work

This study focused on the structural and gas-coupling behaviors of aggregates grown using several different aspect ratios for two types of ellipsoidal grains. Results from this work can be applied to numerical simulations of aggregation, such as those which employ the Smoluchowski equation (Ossenkopf 1993). Solutions to such simulations would provide further insight into how the presence of ellipsoidal grains in astrophysical environment may alter the evolution of large dust populations, such as those that are found in PPDs.

While this work has focused on aggregate growth in the hit-and-stick regime, it has been established by numerous studies that restructuring and fragmentation play an integral part in particle growth in PPDs (Chokshi *et al* 1993, Dominik and Tielens 1997, Blum and Wurm 2008, Suyama *et al* 2008, Wada *et al* 2008). Determination of the probabilities of collisions which do not result in pure sticking are known to depend highly upon the collisional energies (determined in part by the friction time), the area of contact between monomers (determined by the geometry of the grains) and the surface chemistry of the grains themselves. Ellipsoidal grains are less symmetric than their spherical counterparts, due to the variation of curvature of their surface. Therefore, it would be useful to examine how the limits of restructuring and fragmentation are altered by use of non-spherical monomers based on commonly assumed astrophysical parameters.

Within the radiative plasma environment of a PPD, it is possible for grains to become charged due to incident currents of ions and electrons. It has been shown that the resulting electrostatic interactions affect not only the coagulation rates but also the morphology of the resulting aggregates (Okuzumi 2009, Matthews *et al* 2012). An extension of this current work which examines the charging of ellipsoidal grains is ongoing.

Acknowledgment

This work was supported by NSF grant no. #0847127.

References

Armitage P J 2010 *Astrophysics of Planet Formation* (Cambridge: Cambridge University Press)
Bardeen C, Toon O, Jensen E, Marsh D and Harvey V 2008 *J. Geophys. Res.* **113** 17202
Baumgarten G, Fiedler J and von Cossart G 2007 *Adv. Space Res.* **40** 772
Blum J and Wurm G 2008 *Annu. Rev. Astron. Astrophys.* **46** 21
Bridges F, Supulver K, Lin D, Knight R and Zafra M 1996 *Icarus* **123** 422
Chokshi A, Tielens A and Hollenbach D 1993 *Astrophys. J.* **407** 806
Dominik C and Nubold H 2002 *Icarus* **157** 173
Dominik C and Tielens A G G M 1997 *Astrophys. J.* **480** 647
Donev A *et al* 2004 *Science* **303** 990
Dullemond C and Dominik C 2005 *Astron. Astrophys.* **434** 971
Gabrielli P *et al* 2004 *Lett. Nature* **432** 1011
Hage H I and Greenberg J M 1990 *Astrophys. J.* **361** 251
Keesee R 1989 *J. Geophys. Res.* **94** 14683
Kouchi A, Kudo T, Nakano H, Arakawa M and Watanabe N 2002 *Astrophys. J.* **566** L121
Martin P G and Whittet D C B 1990 *Astrophys. J.* **357** 113
Mathis J, Rumpl W and Nordsieck K 1977 *Astrophys. J.* **217** 425
Matthews L S, Hayes R L, Freed M S and Hyde T W 2007 *IEEE Trans. Plasma Sci.* **35** 260
Matthews L, Land V and Hyde T 2012 *Astrophys. J.* **744** 8
Matthews L S and Hyde T W 2004 *IEEE Trans. Plasma Sci.* **32** 586
Matthews L S and Hyde T W 2008 *IEEE Trans. Plasma Sci.* **36** 310
Matthews L S and Hyde T W 2009 *New J. Phys.* **11** 063030
Meakin P 1991 *Rev. Geophys.* **29** 317
Nubold H, Poppe T, Rost M, Dominik C and Glassmeier K 2003 *Icarus* **165** 195
Okuzumi S 2009 *Astrophys. J.* **698** 1122
Okuzumi S, Tanaka H and Sakagami M-a 2009 *Astrophys. J.* **707** 1247
Ormel C and Cuzzi J 2007 *Astron. Astrophys.* **466** 413
Ossenkopf V 1993 *Astron. Astrophys.* **280** 617
Ossenkopf V and Henning T 1994 *Astron. Astrophys.* **291** 943
Paszun D and Dominik C 2009 *Astron. Astrophys.* **507** 1023
Perry J, Gostomski E, Matthews L S and Hyde T W 2012 *Astron. Astrophys.* **539** A99
Perry J, Matthews L S and Hyde T W 2010 *IEEE Trans. Plasma Sci.* **38** 792
Suyama T, Wada K and Tanaka H 2008 *Astrophys. J.* **684** 1310
Suyama T, Wada K, Tanaka H and Okuzumi S 2012 *Astrophys. J.* **753** 115
Wada K, Tanaka H, Suyama T, Kimura H and Yamamoto T 2007 *Astrophys. J.* **661** 320
Wada K, Tanaka H, Suyama T, Kimura H and Yamamoto T 2008 *Astrophys. J.* **677** 1296
Wada K, Tanaka H, Suyama T, Kimura H and Yamamoto T 2009 *Astrophys. J.* **702** 1490
Wada K, Tanaka H, Suyama T, Kimura H and Yamamoto T 2011 *Astrophys. J.* **737** 36